Accurate calculation of path-length variation due to intrabeam scattering for an electron beam traversing a lattice

Zhilong Pan,* Wenxuan Wu, Jingyuan Zhao, and Chuanxiang Tang
Department of Engineering Physics, Tsinghua University, Beijing 100084, China and Key Laboratory of Particle and Radiation Imaging, Tsinghua University, Beijing, China

Xiujie Deng and Alexander Wu Chao
Institute for Advanced Study, Tsinghua University, Beijing, China

(Received 22 April 2026; accepted 17 August 2026; published 1 September 2026)

In future storage rings, precise control of the electron-beam phase space will become increasingly important. A key challenge in these dynamics is maintaining the lattice's isochronicity, which is crucial for applications such as optical stochastic cooling and steady-state microbunching. In particular, path-length deviations induced by intrabeam scattering (IBS) could limit the performance of steady-state microbunching light sources. In this paper, we present a more accurate formula for calculating the IBS-induced path-length deviation of an electron beam traversing the lattice, which can aid in lattice optimization. Additionally, we have developed a tool to simulate IBS-kick effects on beam dynamics. It can directly compute the IBS equilibrium emittance in storage rings and efficiently evaluate the associated path-length deviations for an electron beam traversing a lattice.

DOI: 10.1103/ljgb-sk8s

I. INTRODUCTION

Intrabeam scattering (IBS) is an important collective phenomenon in accelerator-based light sources, affecting not only electron storage rings but also free electron lasers (FELs). In storage rings, IBS causes the equilibrium emittance to increase as the beam current rises. In FEL facilities, IBS-induced energy-spread growth can affect radiation characteristics even during a single pass with a very high peak beam current. Piwinski [1] and Bjorken and Mtingwa [2] independently derived the first analytical expressions for the IBS-induced emittance growth rate. Subsequent researchers [3–10] developed and simplified these formulas for practical applications. Numerous studies have also conducted Monte Carlo simulations [11–14] to determine the IBS effect for various beam distributions, although this process is naturally time consuming.

Despite the maturity of IBS theory, dedicated tools for specific applications—such as evaluating IBS-induced path-length deviations in transfer lines—remain scarce. Monte Carlo simulations, while feasible, are too time consuming for iterative lattice optimization. To illustrate the need and utility of such tools, we briefly discuss two representative cases below.

The first application we consider is steady-state microbunching (SSMB) light source optimization [15,16]. To achieve coherent radiation at short wavelengths with a high repetition rate, laser modulation is used to compress the electron bunches in storage rings. Since the modulation strength is significant for high-power radiation applications, a demodulation process is required downstream in the lattice after radiation emission. Strict control of path-length deviations between the modulation and demodulation sections is essential to prevent the equilibrium emittance from growing due to imperfect cancellation of energy modulation. For instance, achieving a 1 kW average EUV radiation power requires an rms deviation of roughly 0.1 nm [17]. Various factors, including nonlinearity, intrabeam scattering (IBS), and synchrotron radiation, can cause path-length deviations as electrons travel through the magnetic lattice. Currently, the absence of a fast and accurate simulation tool for IBS-induced path-length deviations clearly indicates a critical gap in current lattice design capabilities.

The second case involves bunching factor decay in echo-enabled harmonic generation FEL [18,19]. In a simplified analysis, Stupakov [20] expresses the bunching factor decay caused by IBS as $\kappa = \exp(-1/2 \int_0^s D(s) k_{\Delta E}^2(s) ds)$, where $D(s) = \frac{d\sigma_\delta^2}{ds}$ represents the IBS diffusion coefficient along the beam path, and $k_{\Delta E}$ is the trajectory in the Fourier frequency domain resulting from the IBS-induced energy

*Contact author: panzl@mail.tsinghua.edu.cn

kick from the initial to the final state. Moreover, $k_{\Delta E}(s) = -R_{56}(s)k_z + k_{\Delta E}(0)$, where k_z is the wave number corresponding to the radiation wavelength, and $R_{56}(s)$ denotes the momentum compaction between the initial and final points. This expression for the bunching factor decay can also be reformulated as $\kappa = \exp(-\frac{(k_z * \Delta_z(s))^2}{2})$, with

$$\Delta_z(s) = \sqrt{\int_0^s R_{56}^2(s)D(s)ds} \tag{1}$$

representing the standard deviation in path-length caused by IBS along the transfer line.

To date, no detailed study has precisely calculated the IBS-induced path-length deviation along the lattice transfer line, largely because no specific requirements have been identified. Equation (1) provides only an approximate estimate since it does not account for the IBS energy kicks from the horizontal and vertical directions. Although the impact of horizontal and vertical IBS energy kicks on path-length deviation is often negligible, it can be significant in certain cases, as demonstrated in the following sections.

In this paper, we present a rapid IBS simulation tool that employs Zenkevich's method [11], in which the IBS momentum kicks are generated via the analytically derived diffusion coefficient from the Fokker-Planck equation. This tool can simulate scenarios such as the IBS equilibrium emittance in storage rings and the path-length deviations caused by IBS in any lattice, by adding kicks to macroparticles at each magnetic element. Our IBS-kick implementation is more precise than that used in ELEGANT [21], see Eq. (10) in Sec. III for details.

The structure of this paper is outlined as follows. Section II presents the analysis and more precise formulas for the path-length deviation caused by IBS. Section III describes a numerical method to simulate the evolution of the electron-beam phase space under IBS kicks as it travels along the lattice. A comparison between the results obtained from the analytical formulas and the simulation method is provided in Sec. IV, where the path-length deviation for a single pass and the equilibrium emittance of a storage ring are also calculated for comparison. Finally, Sec. V offers a brief summary and conclusion.

II. PATH LENGTH DEVIATION INDUCED BY IBS

A. Problem definition

In the SSMB lattice design, a key challenge is preserving the isochronicity of the lattice between the energy modulation section (M1 in Fig. 1) and the demodulation section (−M1 in Fig. 1), as illustrated in Fig. 1.

Certainly, numerous factors can disrupt the isochronous condition, and these must be carefully mitigated in our lattice design. A particularly critical factor is IBS. Figure 2 illustrates how IBS induces path-length deviation for a particle.

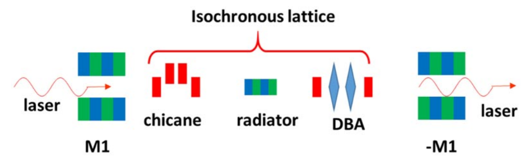

FIG. 1. Sketch of SSMB insertion lattice between modulation and demodulation.

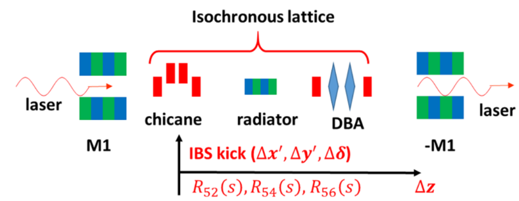

FIG. 2. The path-length deviation induced by IBS.

At any position s along the lattice, an IBS collision imparts a momentum kick to the particle, represented by $(\Delta x', \Delta y', \Delta\delta)$. These kicks are mutually independent, both among particles and at different locations. We define the phase space coordinates of the electron beam as $(x, x', y, y', z, \delta)$ and decompose x and x' into betatron motion and dispersive motion as follows

$$x = x_\beta + \eta_x\delta \quad x' = x'_\beta + \eta'_x\delta, \tag{2}$$

where x_β, x'_β are contributed from the betatron motion, η_x, η'_x are dispersion and dispersion angle.

Then, the momentum kicks caused by IBS will result in a deviation in the path length as

$$\begin{aligned}\Delta z(s) = R_{56}(s) * \Delta\delta + R_{52}(s) * \Delta x' \\ + o(\Delta\delta^2) + o(\Delta x'^2) + o(\Delta\delta\Delta x').\end{aligned} \tag{3}$$

The terms $R_{56}(s)$ and $R_{52}(s)$ denote the transfer coefficients from the collision point s to the lattice's endpoint. The subscripts in $R_{56}(s)$ and $R_{52}(s)$ indicate the row and column elements of the transfer matrix. The high order terms o$(\Delta\delta^2)$, o$(\Delta x'^2)$, and o$(\Delta\delta\Delta x')$ come from high order transfer matrix elements T_{566}, T_{522}, and T_{562}, respectively. In most cases, they can be omitted. Because the momentum kick induced by IBS is much smaller than the beam relative energy spread in most cases (for example, at the order of 1×10^{-5}), then the $T_{566}\Delta\delta$ ($T_{522}\Delta x'$) is much smaller than $R_{56}(R_{52})$ except some special cases. So we omitted high order terms in later discussion. In this context, we assume the absence of any vertical bending magnets, which means that $R_{54} = 0$ at every point within the lattice.

The overall deviation in path length can then be calculated by integrating it along the lattice

$$\Delta z_t = \int_0^{s_e} \Delta z(s) ds = \int_0^{s_e} (R_{56}(s) * \Delta\delta + R_{52}(s) * \Delta x') ds, \tag{4}$$

where s_e represents the total length of the lattice. The induced path length is random for particles within the beam because of the random IBS kicks. These kicks lead to imperfect cancellation of particle momentum between modulation and demodulation, causing the energy spread to increase turn by turn. Further details are available in Ref. [17].

B. Detailed calculation

We assume the IBS kicks are uncorrelated both along the lattice and among particles. Therefore, the root mean square (rms) value of Δz_t can be determined by first averaging over all kicks for the beam at a given location, and then integrating over all locations. The resulting expression is given as follows

$$\begin{aligned}\sigma^2_{\Delta z_t} &= \int_0^{s_e} R_{56}(s)^2 \frac{\langle \Delta\delta\Delta\delta\rangle}{cdt} ds + \int_0^{s_e} R_{52}(s)^2 \frac{\langle \Delta x'\Delta x'\rangle}{cdt} ds + \int_0^{s_e} 2R_{52}(s)R_{56}(s) \frac{\langle \Delta\delta\Delta x'\rangle}{cdt} ds \\ &\text{with} \\ \sigma^2_{\Delta z_t 66} &= \int_0^{s_e} R_{56}(s)^2 \frac{\langle \Delta\delta\Delta\delta\rangle}{cdt} ds \\ \sigma^2_{\Delta z_t 22} &= \int_0^{s_e} R_{52}(s)^2 \frac{\langle \Delta x'\Delta x'\rangle}{cdt} ds \\ \sigma^2_{\Delta z_t 26} &= \int_0^{s_e} 2R_{52}(s)R_{56}(s) \frac{\langle \Delta\delta\Delta x'\rangle}{cdt} ds.\end{aligned} \tag{5}$$

Here, c represents the speed of light. The IBS diffusion coefficient can be expressed as a matrix D,

$$D = \begin{bmatrix} \frac{\langle \Delta x'\Delta x'\rangle}{dt} & \frac{\langle \Delta x'\Delta y'\rangle}{dt} & \frac{\langle \Delta x'\Delta\delta\rangle}{dt} \\ \frac{\langle \Delta x'\Delta y'\rangle}{dt} & \frac{\langle \Delta y'\Delta y'\rangle}{dt} & \frac{\langle \Delta y'\Delta\delta\rangle}{dt} \\ \frac{\langle \Delta x'\Delta\delta\rangle}{dt} & \frac{\langle \Delta\delta\Delta y'\rangle}{dt} & \frac{\langle \Delta\delta\Delta\delta\rangle}{dt} \end{bmatrix}. \tag{6}$$

The element in the matrix D is denoted as D_{ij}. Once the IBS diffusion coefficient is determined, the problem is completely resolved.

In storage rings, we typically calculate the emittance growth rate caused by IBS as [7],

$$\begin{aligned}\frac{1}{T_x} &= \frac{d\epsilon_x}{\epsilon_x dt} \\ &= \frac{\beta_x}{2\epsilon_x} D_p(1,1) - 2\frac{\beta_x\gamma\phi_x}{2\epsilon_x} D_p(1,3) + \frac{\gamma^2\mathcal{H}_x}{2\epsilon_x} D_p(3,3) \\ \frac{1}{T_y} &= \frac{d\epsilon_y}{\epsilon_y dt} \\ &= \frac{\beta_y}{2\epsilon_y} D_p(2,2) \\ \frac{1}{T_z} &= \frac{d\sigma_p^2}{\sigma_p^2 dt} \\ &= \frac{\eta_x^2}{2\sigma_s^2} D_p(1,1) + \frac{\gamma^2}{2\sigma_p^2} D_p(3,3),\end{aligned} \tag{7}$$

with

$$D_p = \begin{bmatrix} \frac{\Delta\langle x'x'\rangle}{dt} & \frac{\Delta\langle x'y'\rangle}{dt} & \frac{\Delta\langle x'\delta\rangle}{dt} \\ \frac{\Delta\langle x'y'\rangle}{dt} & \frac{\Delta\langle y'y'\rangle}{dt} & \frac{\Delta\langle y'\delta\rangle}{dt} \\ \frac{\Delta\langle x'\delta\rangle}{dt} & \frac{\Delta\langle \delta y'\rangle}{dt} & \frac{\Delta\langle \delta\delta\rangle}{dt} \end{bmatrix}, \tag{8}$$

here, T_x, T_y, and T_z represent the horizontal, vertical, and longitudinal IBS growth times, respectively, in the context of storage rings. The symbol ϵ_x denotes the horizontal beam emittance, ϵ_y the vertical beam emittance, σ_s the bunch length, σ_p the relative energy spread, and γ the Lorentz factor. It is important to note that there is a slight difference between D and D_p; further details can be found in Eq. (11).

$$\phi_x = \eta'_x + \frac{\alpha_x\eta_x}{\beta_x} \qquad \mathcal{H}_x = \gamma_x\eta_x^2 + 2\alpha_x\eta_x\eta'_x + \beta_x\eta'^2_x, \tag{9}$$

and the horizontal Twiss parameters are denoted by β_x, α_x, and γ_x.

Analytical expressions for all the components of D_p and D are available for Gaussian beams, as reported in Refs. [7,11]. The resulting IBS-induced path-length deviation can be evaluated directly using Eqs. (5) and (6). Moreover, in the following section we propose a faster simulation method to cross-check the outcomes of Eq. (5).

III. SIMULATION METHOD

To benchmark the analytical results of Eq. (5) and to provide a versatile tool for arbitrary lattices, we implement a simulation based on Zenkevich's method [11]. Unlike the lumped-kick approach in ELEGANT [21], which is designed primarily for equilibrium emittance, our method applies local kicks per magnet element to accurately resolve path-length variations.

A. The method in ELEGANT

Before explaining our simulation procedure, we provide a brief overview of the simulation approach used in ELEGANT [21]. In ELEGANT, an element called IBSCATTER serves as the IBS simulator. To simulate the equilibrium emittance affected by IBS in storage rings, multiple IBSCATTER elements need to be placed along the lattice. ELEGANT computes the integrated IBS growth rates between any two IBSCATTER elements and applies momentum kicks to the particles based on these growth rates each time they reach an IBSCATTER element.

Taking horizontal direction for an example, the amplitude of momentum kick to be added should be

$$\begin{aligned}\sigma^2_{\Delta x'} &= \frac{2d\epsilon_x}{\beta_x dt}\Delta t = \frac{2\epsilon_x}{\beta_x T_x}\Delta t \\ &= \Delta t\left(D_p(1,1) - 2\gamma\phi D_p(1,3) + \frac{\gamma^2\mathcal{H}_x}{\beta_x}D_p(3,3)\right).\end{aligned} \tag{10}$$

Here, $\Delta t = ds/c$ represents the time interval between any two IBSCATTER elements, with ds the distance between any two IBSCATTER. It is important to note that the amplitude of the momentum kick in Eq. (10) does not correspond to the actual momentum kick of D_{11} as defined in Eq. (5). Instead, it includes matrix transfer effects through $D_p(1,3)$ and $D_p(3,3)$. By inserting a limited number of IBSCATTER elements at dispersion-free points within the storage ring lattice, one can obtain accurate equilibrium emittance results using the ELEGANT simulation method. To precisely determine the path-length deviation caused by the IBS kick, a reliable approach is to compute the local D_{ij} at each magnet, then apply momentum kicks with amplitudes derived from these D_{ij} values, updating particle coordinates accordingly through kicks and matrix transformations at every magnet step. Further details are provided below.

B. Our method to add IBS kick

In this paper, we use the approach proposed by Zenkevich [11]. By defining $P = (x', y', \delta)$, the components of the matrix D_p can be separated into a damping part and a diffusion part as follows

$$\begin{aligned}D_p(i,j) &= \left\langle\frac{d(P_iP_j)}{dt}\right\rangle \\ &= -(K_i + K_j)\langle P_iP_j\rangle\delta_{ij} + \langle D_{ij}\rangle.\end{aligned} \tag{11}$$

Here, δ_{ij} represents the delta function, and the quantities K_i and D_{ij} can be determined using the Bjorken-Mtingwa model [11]. Assuming the beam distribution is Gaussian, then the coefficients of K_i and D_{ij} in a planar storage ring at any location can be expressed as below.

$$\begin{aligned}K_1 &= \frac{\beta_x T_{xx}}{\epsilon_x} \\ K_2 &= \frac{\beta_y T_{yy}}{\epsilon_y} \\ K_3 &= \frac{\gamma^2 T_{zz}}{\sigma_p^2} \\ D_{11} &= T_{yy} + T_{zz} \\ D_{22} &= T_{xx} + T_{zz} \\ D_{33} &= \gamma^2 T_{xx} + \gamma^2 T_{yy} \\ D_{13} &= \gamma T_{xz}.\end{aligned} \tag{12}$$

Here, the subscript 1 represents x direction, 2 represents y direction, and 3 represents z direction. The elements not shown above in D_{ij} are all zero in a planar storage ring. And

$$\begin{aligned}T_{xx} &= 4\pi A_0(\log)\left(\frac{a_0 - b_0 + m_0}{2m_0}g_1 + \frac{b_0 - a_0 + m_0}{2m_0}g_3\right) \\ T_{yy} &= 4\pi A_0(\log)g_2 \\ T_{zz} &= 4\pi A_0(\log)\left(\frac{a_0 - b_0 + m_0}{2m_0}g_3 + \frac{b_0 - a_0 + m_0}{2m_0}g_1\right) \\ T_{xz} &= 4\pi A_0(\log)\frac{3d_0}{2m_0}(g_1 - g_3).\end{aligned} \tag{13}$$

Here, (log) represents the Coulomb log factor.

$$A_0 = \frac{r_0^2 cN}{16\pi^2\gamma^4\epsilon_x\epsilon_y\sigma_s\sigma_p}. \tag{14}$$

r_0 is the classical electron radius, N is the number of electrons in the bunch. $a_0 = 1 + \frac{\eta_x^2\epsilon_x}{\sigma_s^2\beta_x}$, $b_0 = \frac{\gamma^2(\epsilon_x + \mathcal{H}_x\sigma_p^2)}{\beta_x\sigma_p^2}$, $d_0 = -\gamma\phi_x$, $m_0 = \sqrt{(b_0 - a_0)^2 + 4d_0^2}$ [10]. And g_1, g_2, g_3 can be expressed as below [7,10]

$$\begin{aligned}g_1 &= \int_0^{\pi/2}\frac{2t_1\sin^2(s)\cos(s)\mathrm{d}s}{\sqrt{(\sin^2(s) + \frac{t_1}{t_2}\cos^2(s))(\sin^2(s) + \frac{t_1}{t_3}\cos^2(s))}} \\ g_2 &= \int_0^{\pi/2}\frac{2t_2\sin^2(s)\cos(s)\mathrm{d}s}{\sqrt{(\sin^2(s) + \frac{t_2}{t_1}\cos^2(s))(\sin^2(s) + \frac{t_2}{t_3}\cos^2(s))}} \\ g_3 &= \int_0^{\pi/2}\frac{2t_3\sin^2(s)\cos(s)\mathrm{d}s}{\sqrt{(\sin^2(s) + \frac{t_3}{t_1}\cos^2(s))(\sin^2(s) + \frac{t_3}{t_2}\cos^2(s))}},\end{aligned} \tag{15}$$

with $t_1 = \frac{1}{u_1}$, $t_2 = \frac{1}{u_2}$, $t_3 = \frac{1}{u_3}$ and

$$\begin{aligned} u_1 &= \frac{\beta_x}{2\epsilon_x}(a_0+b_0+m_0) \\ u_2 &= \frac{\beta_y}{\epsilon_y} \\ u_3 &= \frac{\beta_x}{2\epsilon_x}(a_0+b_0-m_0). \end{aligned} \tag{16}$$

Once K_i and D_{ij} are computed analytically at any given position, random momentum kicks can be applied to the macroparticles as follows

$$P_i(t+\Delta t) = P_i(t) - K_i P_i(t)\Delta t + \sqrt{\Delta t}\sum_{j=1}^{3} C_{i,j}\xi_j. \tag{17}$$

The variables ξ_1, ξ_2, and ξ_3 are three independent standard normal random variables. The term $C_{i,j}$ is associated with the diffusion coefficient and will be defined later. The symbol Δt represents the time interval corresponding to the length ΔL of the magnet, with $\Delta t = \Delta L/(\beta c)$.

In a planar storage ring, there is generally no coupling between the pairs (x,y) and (y,δ), which means that $C_{2,j}=0$ for all $j\neq 2$. By assuming that $C_{3,1}=0$ and comparing Eq. (11) with Eq. (17), the remaining coefficients $C_{i,j}$ can be determined as follows

$$\begin{aligned} C_{2,2} &= \sqrt{D_{22}} \\ C_{3,3} &= \sqrt{D_{33}} \\ C_{1,3} &= \frac{1}{C_{3,3}}\left(\left\langle\frac{d(P_1P_3)}{dt}\right\rangle + (K_1+K_3)\langle P_1P_3\rangle\right) = \frac{D_{13}}{C_{3,3}} \\ C_{1,1} &= \sqrt{D_{11}-C_{1,3}^2}. \end{aligned} \tag{18}$$

IV. COMPARISON OF SIMULATION AND ANALYTICAL RESULTS

A. Comparison for equilibrium emittance in storage rings

1. Without IBS, lumped synchrotron radiation in storage ring

First, we simulated the evolution of the equilibrium emittance by combining the effects of synchrotron radiation damping and quantum excitation, as shown in Fig. 3(a).

We begin by generating a bunch with a coordinate size of $6\times N_e$, where N_e represents the number of macroparticles. The coordinate vector is denoted as X, and for each particle, the coordinate vector is expressed as $\vec{x} = (x, x', y, y', z, \delta)$. The simulation for each turn is performed in two steps. First, we update the coordinates using $X = R\times X$, where R is the one-turn transfer matrix. Second, we apply the radiation kick to the components $p = (x', y', \delta)$. For each component, the kick is applied as $p = p - pT_0/\tau + \sigma\xi$, where T_0 is the revolution period, τ is the radiation damping time, σ is the amplitude of radiation diffusion, and ξ is a random variable drawn from a standard normal distribution.

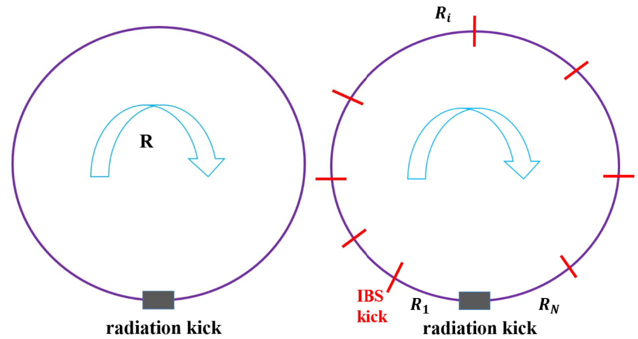

(a) Simulation scheme for lumping synchrotron radiation. (b) Simulation scheme with IBS and lumping synchrotron radiation.

FIG. 3. Simulation scheme in storage rings. (a) Only lumped synchrotron included and linear matrix transformation are included. (b) Lumped synchrotron radiation, linear matrix transformation and IBS kicks are included.

We simulated the ring for 15,000 turns, considering that the ring's damping time is approximately 6000 turns. In this simulation, we used 10,000 macroparticles. The ring parameters are listed in Table I. The evolution of the emittance is illustrated in Fig. 4. As shown in Fig. 4, the simulated equilibrium emittance closely matches the theoretical prediction.

2. With IBS, lumped synchrotron radiation in storage ring

Figure 3(b) illustrates the simulation scheme when IBS is taken into account. The ring is divided into N segments (usually, each segment corresponds to a magnet or a drift space). The coordinates are first transformed by $X = R_i X$, followed by IBS kicks at the ith segment. The IBS kick is applied locally according to Eq. (17). Here, R_i represents the transfer matrix of the ith segment. After completing the tracking through all N segments, the radiation kick is applied as described earlier.

TABLE I. Parameters of the storage ring we used for simulation.

Parameters	Values	Units
Beam energy E_0	2	GeV
Circumference C_0	165.62	m
Natural emittance ϵ_0	27.20	nm
Phase slippage factor η_c	4.32×10^{-7}	…
Tunes ν_x/ν_y	16.213/14.188	…
Relative energy spread σ_δ	1.15×10^{-3}	…
Bunch length σ_z	0.13	mm
Damping times $\tau_x/\tau_y/\tau_z$	3.4/3.4/1.7	ms
Energy loss per turn U_0	0.643	MeV

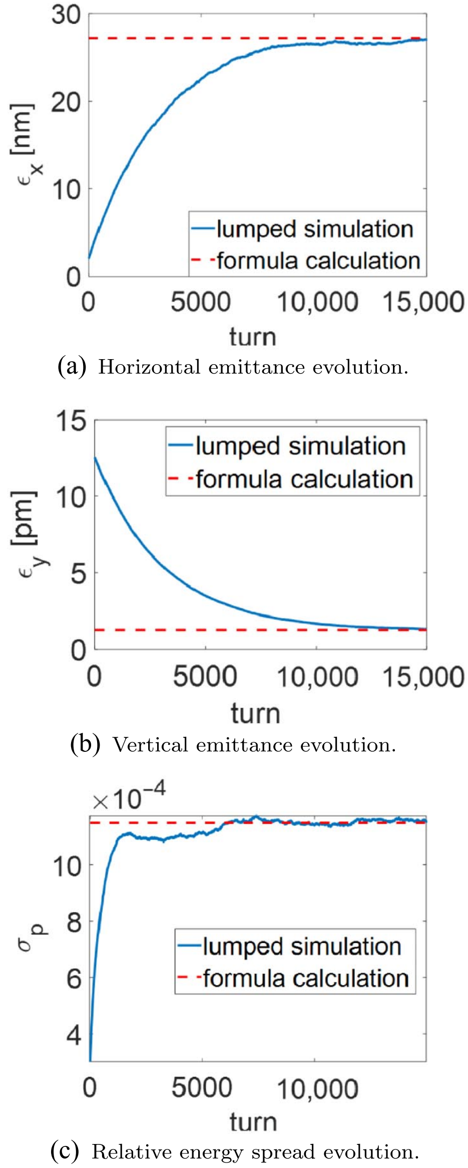

(a) Horizontal emittance evolution.

(b) Vertical emittance evolution.

(c) Relative energy spread evolution.

FIG. 4. The emittance evolution in a storage ring, with only synchrotron radiation is added, with (a) the horizontal emittance evolution (b) the vertical emittance evolution and (c) the relative energy spread evolution. The results from formula calculation are calculated by the classical formulas of equilibrium emittance and relative energy spread when only synchrotron radiation is considered. The readers can refer to Ref. [22].

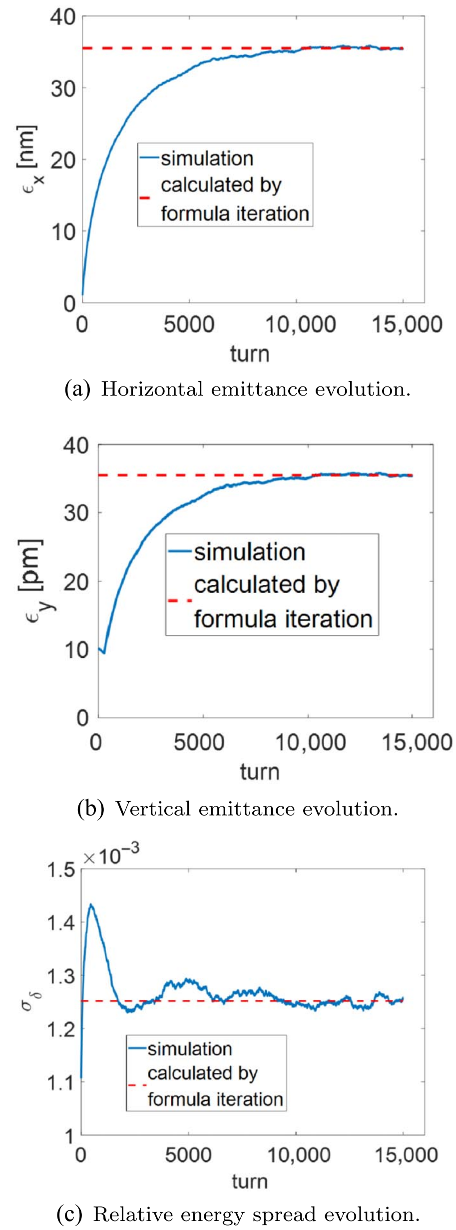

(a) Horizontal emittance evolution.

(b) Vertical emittance evolution.

(c) Relative energy spread evolution.

FIG. 5. The emittance evolution in a storage ring, with synchrotron radiation and IBS kick is added, with (a) the horizontal emittance evolution (b) the vertical emittance evolution and (c) the relative energy spread evolution. The analytical equilibrium emittance with IBS is calculated by iteration method.

The simulation was conducted for 15,000 turns using the ring described earlier. The number of macroparticles was set to 10,000. The results are presented in Fig. 5. The analytical equilibrium emittance with IBS is calculated by iteration method, while the iterative formula used can be found in Ref. [10] of Eq. (14). The relative error between the tracking data and the formula calculation is provided in Table II. The average beam current was approximately 5 A in this case to clearly observe a notable increase in the equilibrium emittance. The horizontal-vertical coupling is set to 0.1% in the tracking simulation and analytical calculation.

The results demonstrate strong consistency between the simulation and the analytical calculation, offering a fast and dependable method for simulating the IBS equilibrium emittance in storage rings.

B. Comparison for single-pass path-length deviation in an isochronous lattice of SSMB insertion

As mentioned in Sec. II, maintaining the isochronous condition of the lattice between modulation and reverse modulation is a crucial aspect in the design of the SSMB

TABLE II. Equilibrium emittance with IBS.

Parameters	Tracking	Calculation	Relative error (%)
ϵ_x[nm]	35.401	35.506	−0.30
ϵ_y[pm]	35.401	35.506	−0.30
$\sigma_\delta[10^{-3}]$	1.257	1.252	0.40

light source. To achieve a high-average EUV radiation power of around 1 kW, the lattice's isochronous condition must be controlled to approximately 0.1 nm [17]. The existing tools (for example ELEGANT) cannot support the accurate calculation and benchmark of the path-length deviation induced by IBS, as also discussed in Sec. III A. The Eq. (5) we derived can be used in the calculation and optimization of such application in SSMB, while the application of Zenkevich's method can be used as a simulation tool for benchmark with our analytical results.

In the design of SSMB light source with high-average EUV radiation power, the lattice with isochronous condition of approximately 0.1 nm is needed. The nonlinear dynamics and IBS effects are two main issues that affect the isochronous condition. So, when we optimize the lattice, we define the two objectives to be minimized as the path-length deviation induced by nonlinear dynamics and IBS. The objective of nonlinear dynamics can be meticulously optimized using the approach described in Ref. [23]. The objective of IBS can be calculated by Eq. (5) in any lattice. In detail, we can calculate the IBS diffusion rates by analytical formula in each element one by one first, then calculate the local $R_{56}(s)$ and $R_{52}(s)$ from the location of this element to the end of the lattice, and finally calculate the contribution to path-length deviation by integration for all elements.

We obtain the optimal solution after above optimization. The lattice's Twiss functions of the optimal solution are displayed in Fig. 6, and the beam parameters are provided in Table III.

Based on Eq. (5), the IBS-induced rms path-length deviation for the lattice is $\sigma_{\Delta z} = 0.1818$ nm, with all the components in Eq. (5) listed below.

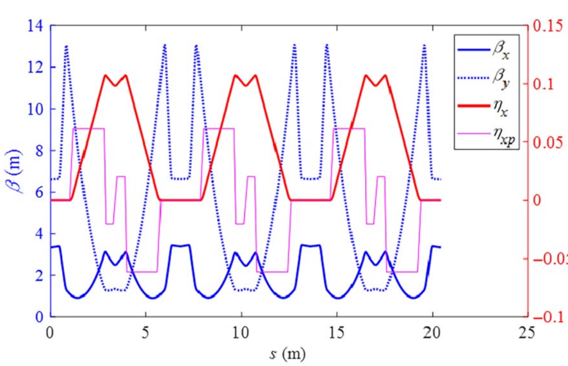

FIG. 6. The Twiss functions of SSMB isochronous lattice.

TABLE III. Parameters of the beam for SSMB isochronous lattice.

Parameters	Values	Units
Beam energy E_0	600	MeV
Horizontal emittance ϵ_x	1	nm
Vertical emittance ϵ_y	1	nm
Relative energy spread σ_δ	1.56×10^{-3}	⋯
Bunch length σ_z	6	mm
Bunch charge	2	nC

TABLE IV. The IBS-induced path-length deviation by simulation.

Macro particle number	$\sigma_{\Delta z}$ (nm)
1000	0.1883
10,000	0.1858
1,00,000	0.1822

$$\begin{aligned} \sigma^2_{\Delta z_t,66} &= 2.80 \times 10^{-20}\ \text{nm}^2 \\ \sigma^2_{\Delta z_t,22} &= 4.82 \times 10^{-21}\ \text{nm}^2 \\ \sigma^2_{\Delta z_t,26} &= -2.58 \times 10^{-22}\ \text{nm}^2. \end{aligned} \tag{19}$$

Clearly, the main contribution arises from the longitudinal kick, while the horizontal kick should not be neglected, as is commonly done.

Next, we perform tracking using the method described in Sec. III. To verify convergence, we repeat the simulation with different macroparticle numbers. After completing the simulation, we compute the standard deviation of $z_f - z_0$ as $\sigma_z = \sqrt{\langle (z_f - z_0)^2 \rangle - \langle z_f - z_0 \rangle^2}$. The results are presented in Table IV.

Based on the results shown in Table IV, we can conclude that the path-length deviation obtained from the simulation is $\sigma_{\Delta z} = 0.1822$ nm, which corresponds to an error of $err = \frac{0.1822-0.1818}{0.1818} = 0.22\%$ compared with the analytical result.

We further compare the computational efficiency of the two methods. For the lattice in Fig. 6, the analytical calculation takes about 0.5 s, while the tracking method takes about 1.3 s with 10,000 macroparticles and 4.5 s with 10,0000 macroparticles. We developed the simulation method primarily to benchmark against the analytical formulas, as no reliable tool exists for this purpose as present.

V. CONCLUSION

In this paper, we develop a simulation tool that employs Zenkevich's semi-analytical method to apply IBS kicks locally to particle momenta. It allows for simulation of the equilibrium emittance in storage rings at a computational cost much lower than that of Monte Carlo simulations. More importantly, it enables rapid per-turn calculation of the IBS-induced path-length deviation—a critical quantity for future high-power storage ring light sources. The consistency between the analytical formula and the fast simulation confirms that our method provides a reliable foundation for optimizing the isochronicity in SSMB lattices, where controlling path-length fluctuations to sub-nanometer levels is critical. Our numerical results confirm that this deviation is driven primarily by the longitudinal momentum kick, although the horizontal contribution, often omitted in conventional treatments, proves non-negligible.

ACKNOWLEDGMENTS

This work is supported by the National Key R&D Program of China (Grant No. 2022YFA1603402) and Beijing Natural Science Foundation (Grant No. 1254058), and the Tsinghua University Initiative Scientific Research Program.

DATA AVAILABILITY

There are no publicly available research data or software supporting this manuscript. Requests for further information or data should be sent to the authors.

[1] A. Piwinski, Intra-beam scattering, in *Frontiers of Particle Beams: Proceedings of a Topical Course, Held by the Joint US-CERN School on Particle Accelerators at South Padre Island, Texas, October 23-29, 1986* (Springer, Berlin, Heidelberg, 2005), pp. 297–309.

[2] J. D. Bjorken and S. K. Mtingwa, Intrabeam scattering, Part. Accel. **13**, 115 (1982).

[3] K. Kubo, S. K. Mtingwa, and A. Wolski, Intrabeam scattering formulas for high energy beams, Phys. Rev. ST Accel. Beams **8**, 081001 (2005).

[4] K. L. Bane, A simplified model of intrabeam scattering, arXiv:physics/0206002.

[5] A. Piwinski, Intra-beam scattering in presence of linear coupling, Deutsches Elektronen-Synchrotron (DESY), Technical Report, 1990.

[6] V. Lebedev and S. Nagaitsev, Multiple intrabeam scattering in X-Y coupled focusing systems, arXiv:1812.09275.

[7] K. Kubo and K. Oide, Intrabeam scattering in electron storage rings, Phys. Rev. ST Accel. Beams **4**, 124401 (2001).

[8] B. Nash, Analytical approach to Eigen-emittance in storage rings, Ph.D. thesis, Stanford University, Stanford, 2006.

[9] F. Antoniou, Optics design of intrabeam scattering dominated damping rings, Ph.D. thesis, CERN, 2012.

[10] Z. Pan, W. Huang, C. Tang, X. Deng, and A. W. Chao, Intrabeam scattering study for longitudinal strong focusing storage rings and lattice optimization, Phys. Rev. Accel. Beams **28**, 114201 (2025).

[11] P. Zenkevich, O. Boine-Frankenheim, and A. Bolshakov, A new algorithm for the kinetic analysis of intra-beam scattering in storage rings, Nucl. Instrum. Methods Phys. Res., Sect. A **561**, 284 (2006).

[12] S. Papadopoulou, F. Antoniou, T. Argyropoulos, M. Hostettler, Y. Papaphilippou, and G. Trad, Impact of non-Gaussian beam profiles in the performance of hadron colliders, Phys. Rev. Accel. Beams **23**, 101004 (2020).

[13] A. Vivoli and M. Martini, Intra-beam scattering in the CLIC damping rings, Technical Report, 2010.

[14] P. D. Valdor, A. Latina, and A. Gerbershagen, Intrabeam scattering simulation with a novel hybrid-kinetic Monte Carlo method for linear accelerators, in *32nd Linear Accelerator Conference, LINAC 2024* (JACoW Publishing, Chicago, USA, 2024), pp. 659–662.

[15] D. F. Ratner and A. W. Chao, Steady-state microbunching in a storage ring for generating coherent radiation, Phys. Rev. Lett. **105**, 154801 (2010).

[16] X. Deng, A. Chao, J. Feikes, A. Hoehl, W. Huang, R. Klein, A. Kruschinski, J. Li, A. Matveenko, Y. Petenev *et al.*, Experimental demonstration of the mechanism of steady-state microbunching, Nature (London) **590**, 576 (2021).

[17] X. Deng, Z. Pan, J. Zhao, Z. Li, A. Chao, and C. Tang, "Reversible microbunching in an electron storage ring," Phys. Rev. Accel. Beams (to be published).

[18] D. Xiang and G. Stupakov, Echo-enabled harmonic generation free electron laser, Phys. Rev. ST Accel. Beams **12**, 030702 (2009).

[19] G. Stupakov, Using the beam-echo effect for generation of short-wavelength radiation, Phys. Rev. Lett. **102**, 074801 (2009).

[20] G. Stupakov, Intra-beam scattering and the ultimate seeding wavelength in EEHG in The workshop names SSSFEL12 (seeding and self-seeding at new FEL sources, Trieste, Italy, 10-12 December 2012) (2012), https://www.elettra.eu/SSSFEL12/Main.HomePage.html.

[21] M. Borland, ELEGANT: A flexible SDDS-compliant code for accelerator simulation, Argonne National Lab., IL (US), Technical Report, 2000.

[22] A. W. Chao, *Lectures on Accelerator Physics* (World Scientific, 2020).

[23] Z. Pan, J. Zhao, C. Tang, X. Deng, and A. W. Chao, Isochronous lattice design with time-of-flight fluctuation reaching subattoseconds based on high-order achromat, Phys. Rev. Accel. Beams **28**, 124001 (2025).